

Action correlations and random matrix theory

Uzy Smilansky and Basile Verdene

Department of Physics of Complex Systems, The Weizmann Institute of Science,
Rehovot 76100, Israel

E-mail: uzy.smilansky@weizmann.ac.il and b.verdene@weizmann.ac.il

Received 23 September 2002

Published 12 March 2003

Online at stacks.iop.org/JPhysA/36/3525

Abstract

The correlations in the spectra of quantum systems are intimately related to correlations which are of genuine classical origin, and which appear in the spectra of actions of the classical periodic orbits of the corresponding classical systems. We review this duality and the semiclassical theory which brings it about. The conjecture that the *quantum* spectral statistics are described in terms of random matrix theory, leads to the proposition that the *classical* two-point correlation function is also given in terms of a universal function. We study in detail the spectrum of actions of the Baker map, and use it to illustrate the steps needed to reveal the classical correlations, their origin and their relation to symbolic dynamics.

PACS numbers: 03.65.Sq, 05.45.Mt

1. Introduction

The interest in the correlation between classical periodic orbits, and in particular, in the spectrum of their actions, emerges from the attempts to provide a semiclassical proof of the universality of spectral correlations of quantum chaotic systems ('the BGS conjecture' [1]). Action correlations were first discussed by Argaman *et al* [2] where the universality of action correlations and their relation to random matrix theory (RMT) were studied for a few chaotic systems. Various aspects of the subject were investigated later [3, 4, 6–8, 10, 15]. This culminated recently in the work of Sieber and Richter [12], who identified pairs of correlated trajectories, whose contribution to the spectral form factor for systems with time reversal symmetry is identical to the next-to-leading order term in the form factor predicted by RMT (see also [13, 14]).

The purpose of this paper is twofold. First, to review the semiclassical context where action correlations and their expected universal features arise in a natural way [10, 15]. This will be done in the main body of the present section, where also the connection with RMT will be made explicit. Second, to test the general semiclassical arguments on action correlations

for a paradigm chaotic dynamical system—the Baker map. This system was investigated previously by a number of groups, [2, 3, 6, 8], who demonstrated numerically the existence of the expected correlations. Here, we develop another approach for the analysis of the action spectrum, where we try to systematically assess the way the periodic orbits and their actions can be partitioned into families which are dynamically related. One aspect of this approach is studied by casting the problem as an Ising model (in one dimension and with a long range, yet exponentially decaying interaction). Moreover, we show several features of the action correlations which escaped the attention of previous works, and in particular, we analyse the correlations in terms of the symbolic dynamics. We hope that this insight will pave the way to a more complete understanding of the universal features of action correlations in general.

1.1. Action correlations and the semiclassical theory of spectral statistics

Consider a finite, two-dimensional domain \mathcal{A} and an area preserving map

$$\mathcal{M} : \gamma' = \mathcal{M}(\gamma) \quad \gamma', \gamma \in \mathcal{A}. \quad (1)$$

Any area preserving map can be expressed implicitly through a generating function [16]. Let $\gamma = (x, y)$ and $\gamma' = (x', y')$. The generating function $F_1(x', x)$ defines the map through the relations

$$y = -\frac{\partial F_1(x', x)}{\partial x} \quad y' = \frac{\partial F_1(x', x)}{\partial x'} \quad (2)$$

where x' is to be expressed in terms of (x, y) by solving the first equation, and y' is given explicitly using the second equation. Twist maps are maps for which the first equation above has a unique solution for any $(x, y) = \gamma \in \mathcal{A}$. From now on, we shall assume \mathcal{M} to be a *hyperbolic* twist map.

Periodic points of period n are solutions of the equation $\gamma = \mathcal{M}^n(\gamma)$. The corresponding n -periodic orbit is obtained by iterating the map: $\gamma_0^{(a)}, \gamma_1^{(a)} = \mathcal{M}(\gamma_0^{(a)}), \dots, \gamma_{n-1}^{(a)} = \mathcal{M}^{n-1}(\gamma_0^{(a)})$. The *action* assigned to a periodic orbit is

$$f_a = \sum_{j=1}^n F_1(x_j^{(a)}, x_{j-1}^{(a)}) \quad x_0^{(a)} = x_n^{(a)}. \quad (3)$$

The number of n -periodic orbits N_n increases exponentially with n . The object of our investigations is the set of actions $\{f_a\}_{a=1}^{N_n}$, in the limit $n \rightarrow \infty$.

Under quite general conditions, one can show that the mean action $\langle f \rangle_n$ and the variance $\text{var} f(n)$ are both proportional to n . Moreover, the actions of n -periodic orbits are bounded within an interval which grows *algebraically* with n . However, since their number grows *exponentially* with n , one expects exponentially small spacings between successive actions. We shall explain now why the pair correlations of action are expected to be universal, and determined by RMT. To this end we should address the quantum analogue of the map, in the semiclassical limit.

The quantum analogue of the classical map is a unitary evolution operator U_N which acts on an N -dimensional Hilbert space, with

$$N = \left[\frac{\|\mathcal{A}\|}{2\pi\hbar} \right] \quad (4)$$

where $[\cdot]$ stands for the integer value and $\|\mathcal{A}\|$ is the area of \mathcal{A} .

The spectrum of U_N consists of N unimodular complex numbers $e^{i\theta_l(N)}$, $\theta_l(N) \in [0, 2\pi)$. Ample numerical evidence supports the conjecture that the spectral statistics of U_N is well

reproduced by the predictions of RMT. The quantum spectral density is denoted by

$$d_{qm}(\theta; N) = \sum_{l=1}^N \delta(\theta - \theta_l(N)). \quad (5)$$

In the semiclassical approximation,

$$\langle x' | U_N | x \rangle = \left(\frac{1}{2\pi\hbar i} \right)^{\frac{1}{2}} \left(\frac{\partial^2 F_1(x', x)}{\partial x' \partial x} \right)^{\frac{1}{2}} e^{iF_1(x', x)/\hbar}. \quad (6)$$

Here, x is a discrete index which labels the eigenstates of the position operator and $F_1(x', x)$ is the classical generating function. A detailed discussion of the semiclassical evolution operator and its properties can be found in [5].

The semiclassical approximation (6) yields

$$\int_0^{2\pi} d\theta e^{in\theta} d_{qm}(\theta; N) = \text{Tr} U_N^n \approx \sum_{a \in \mathcal{P}_n} A_a^{(n)} e^{if_a/\hbar + i\frac{\pi}{2} r_a \mu_a} \quad (7)$$

where \mathcal{P}_n is the set of n -periodic orbits. $A_a^{(n)}$ are the stability amplitudes,

$$A_a^{(n)} = \frac{n}{r_a |\det(I - T_a^{r_a})|^{\frac{1}{2}}}. \quad (8)$$

Here, r_a stands for the repetition number if the periodic orbit is a repetition of a primitive n_a -periodic orbit ($n_a = \frac{n}{r_a}$). T_a is the monodromy matrix and μ_a is the Maslov index for the primitive orbit.

At this point, we introduce the *classical* density of actions of n -periodic orbits,

$$d_{cl}(f; n) = \sum_{a \in \mathcal{P}_n} A_a^{(n)} e^{i\frac{\pi}{2} r_a \mu_a} \delta(f - f_a(n)) \quad (9)$$

and we obtain

$$\text{Tr} U_N^n \approx \int df e^{if/\hbar} d_{cl}(f; n). \quad (10)$$

Using (4), and measuring the actions in units of the phase space area $s = f/\|\mathcal{A}\|$, we get the relation between the quantum and the classical densities:

$$\int_0^{2\pi} d\theta e^{iv\theta} d_{qm}(\theta; N) \Big|_{v=n} \approx \int ds e^{iks} d_{cl}(s; n) \Big|_{k=2\pi N}. \quad (11)$$

This equation expresses the quantum–classical duality. It relates two densities which are very different: the quantum density gives a unit weight to all the eigenphases on the unit circle, while in the classical density the actions are weighted by the stability amplitudes, and are assigned with a ‘charge’ ± 1 , $\pm i$ depending on the Maslov index. The duality relation is expressed via a Fourier transform which involves both the variables and the parameters which specify the quantum and the classical distributions. On the quantum side, N is a *parameter* which specifies the value of \hbar , while n is the value of the variable conjugate to θ . On the classical side, n is a *parameter* which specifies the period of the ensemble of orbits under consideration, while N determines the value of k —the variable conjugate to s . In what follows, we shall always reserve the first position for the spectral variable or its conjugate, while the second position is reserved for the parameter which specifies the system.

We shall focus our attention on the spectral form factors, which are the Fourier transforms of the pair correlation functions. The quantum and the classical form factors are given explicitly as

$$K_{qm}(v; N) = \frac{1}{N} \sum_{l, l'=1}^N e^{iv(\theta_l - \theta_{l'})} = \frac{1}{N} \sum_{l, l'=1}^N e^{2\pi i v (\theta_l - \theta_{l'}) \bar{d}_N} \quad (12)$$

where $\tau = \frac{\nu}{N}$, and $\bar{d}_N = \frac{N}{2\pi}$ is the mean density and ν must be an integer since d_{qm} is a periodic function. The classical form factor is

$$K_{cl}(k; n) = \sum_{a, a'=1}^{N_n} A_a^{(n)} A_{a'}^{(n)} e^{i\frac{\pi}{2}(r_a \mu_a - r_{a'} \mu_{a'})} e^{ik(s_a - s_{a'})}. \quad (13)$$

It follows from (11) that the quantum and the classical two-point form factors are related by

$$K_{qm}(\nu = n; N) \approx \frac{1}{N} K_{cl}(k = 2\pi N; n). \quad (14)$$

Hence, the quantum spectral correlations are reflected in the classical spectrum, and vice versa. This equation expresses the important semiclassical result that the quantum form factor is obtained from the classical one by interrogating the spectrum of action differences on the scale of $N^{-1} \sim \hbar$.

Equation (14) has to be understood in the sense of distributions, since the form factors, as defined above, are the Fourier transforms of a sum of δ functions. Indeed, the form factors computed for a given system fluctuate, and do not converge to a limit when $N \rightarrow \infty$. The appropriate way to overcome this difficulty in the present context is to apply a smoothing procedure, which enables the extraction of well-defined limit distributions.

Starting with the quantum form factor, we adopt *spectral averaging* which is based on the assumption of ‘spectral ergodicity’. We order the spectrum so that $\theta_l \leq \theta_{l+1}$, and partition it to N_g subsets σ_g , each consisting of $\hat{N} = \frac{N}{N_g}$ subsequent phases. Neglecting correlations between phases in different subsets, we rewrite (12) as

$$\begin{aligned} K_{qm}(\tau; N) &\approx \frac{1}{N_g} \sum_{g=1}^{N_g} \frac{1}{\hat{N}} \sum_{l, l' \in \sigma_g} e^{i2\pi \tau (\theta_l - \theta_{l'}) \bar{d}_N} \\ &= \frac{1}{N_g} \sum_{g=1}^{N_g} K_{qm}^{(g)}(\tau; \hat{N}). \end{aligned} \quad (15)$$

$K_{qm}^{(g)}(\tau; \hat{N})$ is the form factor for the spectrum obtained by multiplying all $\theta_l \in \sigma_g$ by $\frac{N}{\hat{N}}$ so that they cover the entire circle uniformly. Taking now the limit $N \rightarrow \infty$ at a constant τ , with $N_g \approx \hat{N} \approx \sqrt{N}$, it is expected that $K_{qm}(\tau; N)$, which is expressed now as an average over the ensemble of the partial form factors, converges to a limit distribution $K_{qm}(\tau)$ which reproduces the prediction of RMT for the appropriate ensemble. This procedure is justified by the fact that in the quantum spectrum, the *correlation range* is of the order of a mean spectral spacing. Hence, the elimination of the correlations between different sets in (15) introduces a small error, which vanishes in the large N limit.

A different smoothing procedure is required for the discussion of the classical spectrum. As will be shown in the following, the classical correlation length is of the order of the *inverse* of n which exceeds by far the mean spacing which is exponentially small in n . A spectral smoothing should therefore rely on a different partitioning of the period orbits, such that the relevant correlations are preserved within a subset, while members of different subsets are statistically uncorrelated. One of the main problems in dealing with the classical correlations is the proper definition of such subsets [7]. The smoothing of the classical spectra is by far more important since the number of actions increases exponentially with n .

If we denote the results of the quantum and the classical smoothing procedures by $\langle \cdot \rangle$, we obtain from (14) the relation which is basic to the present approach,

$$\langle K_{qm}(\tau; N) \rangle \approx \frac{1}{N} \left\langle K_{cl} \left(2\pi \frac{n}{\tau}; n \right) \right\rangle \quad \tau = \frac{n}{N}. \quad (16)$$

Assuming that $\langle K_{qm}(n; N) \rangle$ follows the RMT predictions, namely, $\langle K_{qm}(n; N) \rangle = K_{\text{RMT}}(\tau = n/N)$, we find that the classical spectra of chaotic systems must display universal pair correlations which can be derived from RMT using relation (16). In particular, since for large N , $\langle K_{qm}(\tau; N) \rangle$ is a function of τ only, we derive two immediate predictions for $\langle K_{cl}(2\pi \frac{n}{\tau}; n) \rangle$:

- (i) $\langle K_{cl}(2\pi \frac{n}{\tau}; n) \rangle$ is proportional to n , since the right-hand side of (16) must depend on N only through the ratio $\frac{n}{N}$. It is convenient to define

$$\mathcal{K}_n(k) = \frac{1}{n} \langle K_{cl}(k; n) \rangle \quad (17)$$

where the proportionality of $\langle K_{cl}(2\pi \frac{n}{\tau}; n) \rangle$ to n is made explicit.

- (ii) $\mathcal{K}_n(k)$ depends on k only through the scaled variable $\frac{k}{n}$,

$$\mathcal{K}_n(k) = \frac{k}{2\pi n} K_{\text{RMT}}\left(\frac{2\pi n}{k}\right). \quad (18)$$

Since k is the parameter conjugate to the action differences, it follows that the correlation length of the action spectrum is proportional to $\frac{1}{n}$. Moreover, (18) shows that the classical correlations of actions corresponding to different periods are identical up to a scaling, and universal, since they are expressed in terms of a system-independent function. These predictions pertain exclusively to classical properties and, once they are derived within classical mechanics, the road would be cleared for a semiclassical derivation of the BGS conjecture.

The validity of (i) in the limit $\tau \rightarrow 0$ was first shown by Berry [21]. In the present context, it follows from the fact that the actions are discrete variables, and therefore for sufficiently large N the only correlations are the diagonal ones. Hence, for $k \rightarrow \infty$,

$$\langle K_{cl}(k; n) \rangle \rightarrow \sum_a |g_a A_a^{(n)}|^2 \approx n \langle g \rangle \quad (19)$$

where g_a is the number of different orbits which share the same action (mostly due to symmetry) and the summation is now restricted to trajectories with different actions. The equality on the right-hand side is derived by using the ergodic sum-rule [23] and denoting by $\langle g \rangle$ the average value of the g_a . Since $\langle g \rangle$ takes the value 1 for systems without time reversal symmetry, and 2 for systems which are symmetric under time reversal, the leading terms in the RMT results for the CUE and COE are indeed reproduced.

To derive the quantum form factor in a consistent semiclassical way, one has to consider the classical form factor for a fixed n , and change k (or N) so that an interval of τ values is scanned. However, to have meaningful pair correlations, N should be larger than 2, and therefore the range of allowed τ values is at most $0 < \tau < n/2$. A further restriction on the range of τ is due to the limited semiclassical accuracy, which is of the order of a mean spacing [22]. In other words, the semiclassical trace formula may have its poles away from the unit circle, thus replacing the sharp δ functions in (5) by spikes with a finite width, of the order of the mean spacing. Therefore, the regime $\tau > 1$ is not expected to be accessible to the semiclassical approximation, and thus the range of applicability reduces further to the domain $n < N$. It is important to note at this point that the required order of operations (keeping n fixed and taking $N \rightarrow \infty$) is consistent with the correspondence principle and the rules of quantum mechanics where the limit $\hbar \rightarrow 0$ is taken at a fixed value of the classical parameters.

In the present work we shall study the Baker map, which will be introduced in the next section. It is a simple dynamical system, for which various properties can be derived analytically, yet it carries the full complexity of the action spectrum, and therefore it is appropriate as a paradigm. In section 3 the spectrum of the actions will be discussed from

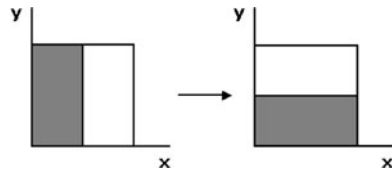


Figure 1. The Baker map.

various points of view, and on the different relevant scales. The expression of the actions in terms of the symbolic codes of the periodic orbits will play a central role. Mapping the computation of the spectral density onto an Ising model enables us to introduce a few approximations which enable the derivation of some properties of the action density (3.3). The classical pair correlations are discussed in section 4. We study first the m th neighbour distributions. We show numerically that as long as m is smaller than the action correlation length $1/n$ measured in units of the mean action spacing, the m th neighbour distributions are essentially Poissonian. Turning to the form factor, we discuss alternative smoothing methods and relate them to the symbolic codes. We finally show that the classical correlations reproduce the expected RMT behaviour as was conjectured in the general discussion presented above. We conclude the paper by a summary, where the connection between the present and previous works is discussed.

2. The Baker map

2.1. The mapping

The Baker map is one of the simplest examples of chaotic maps [17–19]. It is an area preserving map of the unit square onto itself defined by

$$x' = 2x - [2x] \quad y' = \frac{1}{2}y + \frac{1}{2}[2x]. \quad (20)$$

The stretching in the x direction and the squeezing in the y direction are responsible for the hyperbolic character of the map, while the ‘cutting and putting on top’ gives the mixing property. Figure 1 shows one iteration of the map.

The action of the map is easily translated to a Bernoulli shift: every phase space point is presented in a binary basis,

$$x = \sum_{i=1}^{\infty} a_i 2^{-i} = 0 \cdot a_1 a_2 a_3 \dots$$

$$y = \sum_{i=1}^{\infty} b_i 2^{-i} = 0 \cdot b_1 b_2 b_3 \dots$$

with $a_i, b_i \in \{0, 1\}$. The dynamics is given by shifting the binary point to the right when the two fractions are put back to back

$$\dots b_3 b_2 b_1 \cdot a_1 a_2 a_3 \dots \longrightarrow \dots b_3 b_2 b_1 a_1 \cdot a_2 a_3 \dots$$

$$x = 0 \cdot a_1 a_2 a_3 \dots \longrightarrow x' = 0 \cdot a_2 a_3 \dots$$

$$y = 0 \cdot b_1 b_2 b_3 \dots \longrightarrow y' = 0 \cdot a_1 b_1 b_2 b_3 \dots$$

2.2. Periodic orbits and codes

An n -periodic point is represented as an infinite repetition of a finite binary string with n entries $v = (v_1, v_2, \dots, v_n)$, $v_i \in \{0, 1\}$. The cyclic permutations of $(v_1 \dots v_n)$ represent the periodic points which constitute the periodic orbit. The number of n -periodic orbits is $\approx 2^n/n$. The phase space coordinates of an n -periodic point can be written in terms of the code

$$x_i = \frac{1}{1 - 2^{-n}} \sum_{j=1}^n v_{i+j-1} 2^{-j} \quad y_i = \frac{1}{1 - 2^{-n}} \sum_{j=1}^n v_{i+j-1} 2^{-n+j-1}. \quad (21)$$

As $n \rightarrow \infty$ periodic points fill phase space densely and uniformly.

The symbolic dynamics introduced above is based on the partition of the unit square into two equal rectangles along the line $x = \frac{1}{2}$. The sequence of binary symbols indicates the order in which the orbit visits the rectangles. Alternative codes can be generated by partitioning the unit square along the lines $x_j = j \frac{1}{2^r}$, with $r > 1$ integer and $1 \leq j \leq 2^r - 1$. A symbolic code consisting of the 2^r symbols $0, 1, \dots, 2^r - 1$ indicates the order in which the periodic orbit visits the rectangles. The translation of a binary sequence to the 2^r code is done by considering successive sequences of r binary symbols as integers in $[0, 1, \dots, 2^r - 1]$. (For example, the binary code $\{001110101\}$ is translated to the $2^{r=3}$ code $\{137652524\}$.) Increasing r the code becomes more informative, because it locates the rectangles with an accuracy 2^{-r} along the x -axis. However, this is achieved at a cost: not all sequences of symbols are allowed. They are restricted by a Markovian grammar with a $2^r \times 2^r$ connectivity matrix with only two nonvanishing entries per row.

$$C_{jj'}^{(r)} = \begin{cases} 1 & \text{for } (j' - 2j) \bmod 2^r \in \{0, 1\} \\ 0 & \text{otherwise.} \end{cases} \quad (22)$$

The refined codes will be used in the following.

2.3. Symmetries

The mapping possesses two discrete symmetries [17]. The first is a space reflection symmetry

$$\hat{R}: x \longrightarrow 1 - x \quad \text{and} \quad y \longrightarrow 1 - y.$$

Geometrically, it is a double reflection about both the $y = 1 - x$ diagonal and the $y = x$ diagonal. It manifests itself on the code by $\hat{R}(v_i) = 1 - v_i$. The second is time reversal

$$\hat{T}: x \longrightarrow y \quad y \longrightarrow x \quad \text{and} \quad t \longrightarrow -t$$

where reversing the time means reversing the mapping. Geometrically, it is a reflection about the $y = x$ diagonal and its action on the code of a periodic orbit is $\hat{T}(v_i) = v_{n-i+1}$. Figure 2 shows the action of the symmetry transformations: \hat{R} , \hat{T} and $\hat{R}\hat{T} = \hat{T}\hat{R}$ on the code $v = (0001011)$.

2.4. Generating function, action

The action s associated with a phase space point (x, y) is defined as the generating function $F_1(x, x')$ of the mapping, with $x' = x'(x, y)$. Because of the fact that in the Baker map the x dynamics is independent of y , one has to derive the action by first extracting the generating function $F_2(x, y')$ from the conditions

$$\frac{\partial F_2(x, y')}{\partial x} = y \quad \frac{\partial F_2(x, y')}{\partial y'} = x'$$

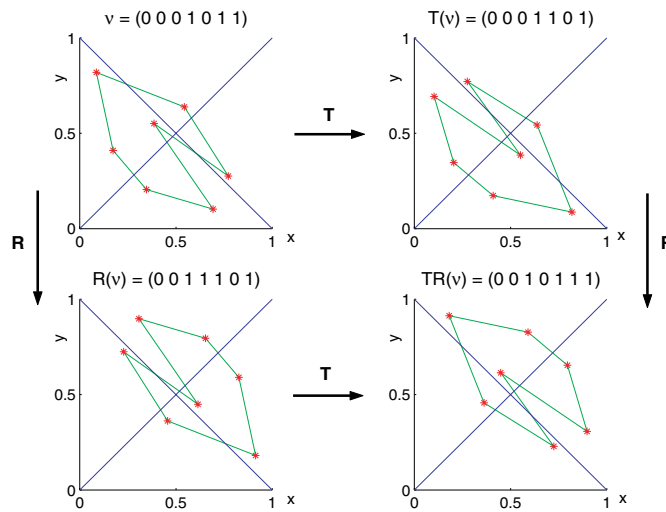


Figure 2. Symmetry related periodic orbits.

and get $F_2(x, y') = 2xy' - x[2x] - y'[2x] + \text{const}$. To obtain $F_1(x, x')$ a Legendre transform is needed (see [25]),

$$F_1(x, x') = F_2(x, y') - x'y' = -x[2x].$$

One should emphasize that $F_1(x, x')$ is not a generating function of the mapping. However choosing $F_1(x, x')$ as the action is consistent with the action obtained from the semiclassical approximation of the quantum Baker map [19, 25]. Adding to the action an integer valued function $I(x)$ does not affect any semiclassical calculation (see [3]). The choice $I(x) = [2x]$ renders the action invariant under the symmetries of the mapping. Inserting an overall minus (a matter of convention) gives $s(x, x') \equiv s(x) = (x - 1)[2x]$. We use the symbol s to denote the actions because the phase space area is $\|\mathcal{A}\| = 1$, so the actions are properly normalized. Applying the above to the i th periodic point (or *segment*) of a periodic orbit ν of length n , yields $s(x_i, x_{i+1}) \equiv s(x_i) = (x_i - 1)[2x_i] = (x_i - 1)v_i$. The total action of the periodic orbit ν is the sum of its *segment* actions,

$$s_n(\nu) = \sum_{i=1}^n s(x_i) = \sum_{i=1}^n (x_i - 1)v_i. \tag{23}$$

The action thus defined is invariant under space reflection \hat{R} , time reversal \hat{T} and the Baker transformation \hat{B} which is only a cyclic permutation of $(v_1 \dots v_n)$, i.e.

$$s_n(\nu) = s_n(\hat{R}(\nu)) = s_n(\hat{T}(\nu)) = s_n(\hat{B}(\nu)). \tag{24}$$

Since the periodic orbits $\nu, \hat{R}(\nu), \hat{T}(\nu), \hat{R}\hat{T}(\nu)$ are not identical in general, one expects a maximal symmetry degeneracy of 4.

The action can also be expressed in a matrix form [8, 20] (see also [9]) which will be useful later. Writing $\langle \nu | = \text{Vec}(v_1 \dots v_n)$ and $|\nu\rangle = \text{Vec}(v_1 \dots v_n)^T$ then the action is

$$s_n(\nu) = \langle \nu | \hat{O} | \nu \rangle - \langle \nu | \nu \rangle \tag{25}$$

where \hat{O} is an $n \times n$ cyclic matrix, with matrix elements

$$O_{ij} = \frac{1}{2^n - 1} 2^{(i-j+n-1) \bmod n}. \tag{26}$$

This expression of the actions clearly shows that their values are restricted to integer multiples of 2^{-n} . This is the minimum separation in the action spectrum.

The Baker map is uniformly hyperbolic. The stability eigenvalues of all the n -periodic orbits are the same, namely $\lambda_{\pm} = 2^{\pm n}$, the corresponding eigenvectors are parallel to the (x, y) -axes, and the Maslov indices are all null. These features bring a large degree of simplification which is to be incorporated in the definition of the action density for the Baker map.

3. The action density

The action density (9) for the Baker map takes the form

$$d_{cl}(s; n) = \frac{1}{2^{\frac{n}{2}} - 2^{-\frac{n}{2}}} \sum_v \delta(s - s(v)) \quad (27)$$

where the summation extends over all the different vectors v . Note that in this way of writing, repetitions are properly weighted. Since the weights in (27) are all positive, it is convenient to normalize the density to unit integral. We shall denote the normalized density by $P_n(s)$, with $\int P_n(s) ds = 1$ (the subscript *cl* is dropped since we shall deal exclusively with the classical spectrum),

$$P_n(s) = \frac{1}{N_n} \sum_{a \in \mathcal{P}_n} \frac{1}{r_a} \delta(s - s_a) \quad (28)$$

where \mathcal{P}_n stands for the set of distinct n -periodic orbits and r_a is the repetition number. The normalization factor N_n , the number of n -periodic orbits, tends to $\frac{2^n}{n}$ in the large n limit. An alternative expression is obtained by lumping together all the orbits which have the same action and the set $\tilde{\mathcal{P}}_n$ consists of single representatives from each degeneracy set, and g_a is the corresponding degeneracy,

$$P_n(s) = \frac{1}{N_n} \sum_{a \in \tilde{\mathcal{P}}_n} \frac{g_a}{r_a} \delta(s - s_a). \quad (29)$$

As defined in (28), (29), $P_n(s)$ is a distribution. For some purposes, it is advantageous to use a smooth version obtained by convoluting (28), (29) with a narrow window function. The resulting smooth function will also be denoted as $P_n(s)$, and it is shown in figure 3 for $n = 21$.

The simplest (but wrong) estimate for the action density is obtained by assuming that the segment actions $s(x_i) = (x_i - 1)v_i$ (23) are independent random variables which are uniformly distributed on the interval $[-\frac{1}{2}, 0]$. This leads to a Gaussian distribution in the limit of large n , which has the same mean as the action distribution but otherwise is quite different from it. Figure 4 compares the distribution computed numerically for a random choice of segments ($n = 19$), with the actual action distribution (periodic orbits).

We shall start the discussion of the action density by reviewing some general properties. In the next subsection, we shall investigate the substructures in the spectrum, and show that it is partitioned naturally into families which can be characterized in terms of symbolic codes.

3.1. General properties

The action distributions $P_n(s)$ are characterized by various scales whose dependence on n will be summarized below.

Degeneracy in the action spectrum is mainly due to the symmetries (24). As n increases, a larger fraction of the orbits are not self-symmetric, and therefore the mean degeneracy is $\langle g \rangle = 4$. Figure 5 shows the degeneracy distributions for $n = 16, 17$. One can see that for

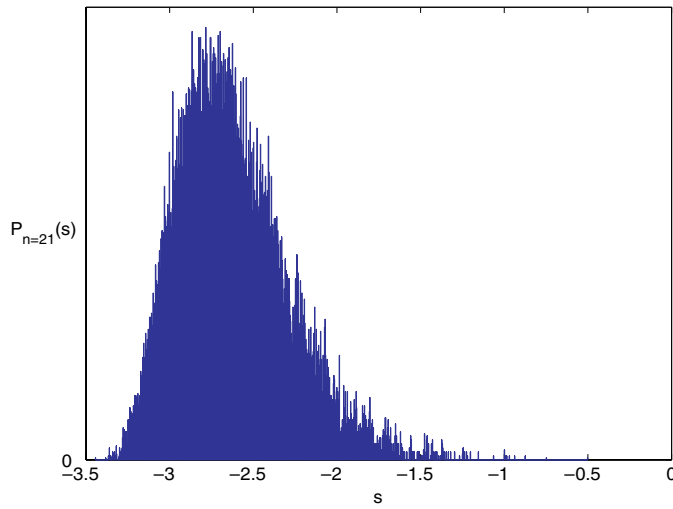


Figure 3. Spectrum of actions, $n = 21$.

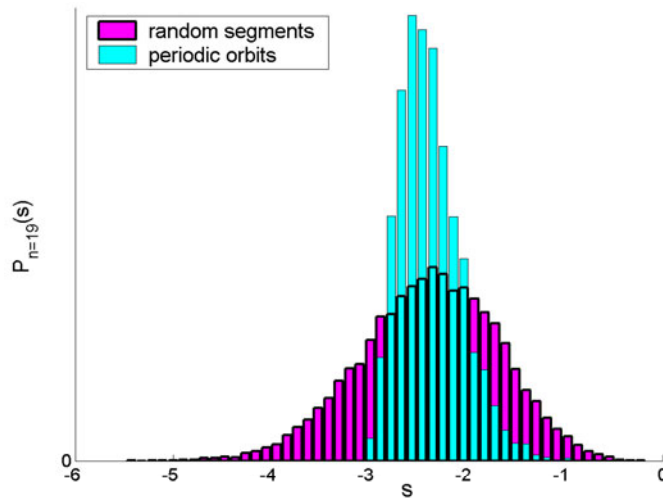


Figure 4. The density of randomly generated actions for $n = 19$, compared with the true density.

these values of n the degeneracies 2 and 1 still appear with appreciable frequency, and higher degeneracies whose origin is number theoretical are also possible.

The lowest scale is 2^{-n} since the actions are integer multiples of this interval.

The largest scale is provided by the interval I_n which supports the action distribution. It follows directly from (25) that the maximum value of s_n is $s_n^{\max} = 0$ while the minimum is given by the action associated with the periodic orbit $\nu = (010101 \dots)$:

$$s_n^{\min} = - \begin{cases} \frac{n}{6} & \text{for } n \text{ even} \\ \frac{n}{6} \left(1 - \frac{1}{3n} \frac{2^n + 1}{2^n - 1}\right) & \text{for } n \text{ odd.} \end{cases} \quad (30)$$

Hence, to leading order $I_n = \frac{n}{6}$. This interval accommodates $N_n \approx \frac{2^n}{n}$ periodic orbits, which are ≈ 4 times degenerate. It follows that *the mean spacing* is

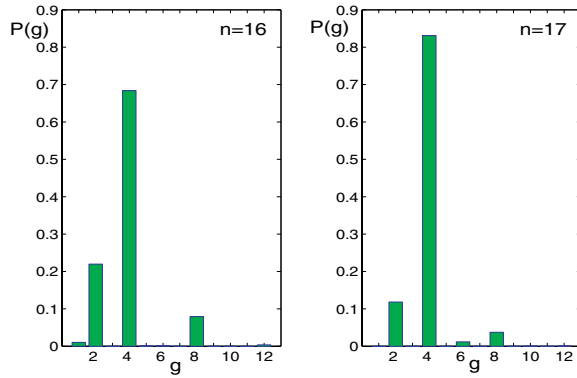


Figure 5. The distribution of degeneracies for $n = 16, 17$.

$$\langle \Delta s^{(n)} \rangle \simeq \frac{2 n^2}{3 2^n}. \tag{31}$$

This estimate reproduces very well the numerical simulations. The above result indicates that not all the integer multiples of 2^{-n} on the action line are populated. Rather, the gaps are of order n^2 . They cannot be seen in figure 3, because the bin size used is too coarse.

To characterize the large scale features of the action distribution, we quote explicitly its first three moments in the limit of large n (the proof of these relations is given in section 3.3 below):

$$\begin{aligned} \langle s_n \rangle &\longrightarrow -\frac{n}{8} \\ \text{var}(s_n) &\longrightarrow \frac{n}{192} \\ \langle (s_n - \langle s_n \rangle)^3 \rangle &\longrightarrow \frac{n}{768}. \end{aligned} \tag{32}$$

To check the limiting action distribution, it is appropriate to examine its dependence on the scaled action:

$$s^* = \frac{s - \langle s_n \rangle}{\sqrt{\text{var}(s_n)}}. \tag{33}$$

Sano [8] has recently shown that the scaled action density becomes Gaussian in the limit of large n . Our numerical computations confirm that

$$\begin{aligned} \lim_{n \rightarrow \infty} \frac{\langle (s_n - \langle s_n \rangle)^l \rangle}{(l-1)! n^{l/2}} &= 1 \quad \text{for } l \text{ even} \\ \lim_{n \rightarrow \infty} \frac{\langle (s_n - \langle s_n \rangle)^l \rangle}{n^{l/2}} &= 0 \quad \text{for } l \text{ odd.} \end{aligned} \tag{34}$$

Figure 6 compares the scaled distributions for $n = 30, 100$, computed for the $r = 5$ level of the Ising model of section 3.3. One can clearly see that the distribution for the larger n gets more symmetric. The fact that the distribution of scaled actions tends to a Gaussian does not imply that pair correlations do not exist.

3.2. Families of actions and symbolic codes

Symbolic codes are naturally associated with a partition of phase space (see e.g. [24]). The actions, being functions of phase space points, are expressed in terms of the codes (25) and

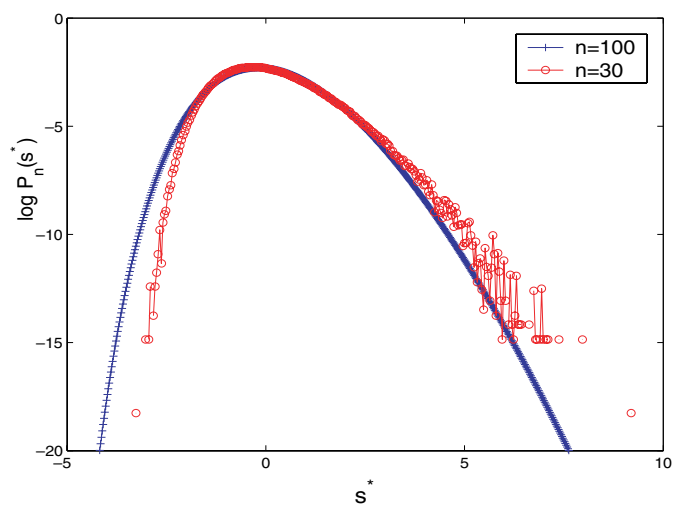


Figure 6. Scaled action densities for $n = 30, 100$.

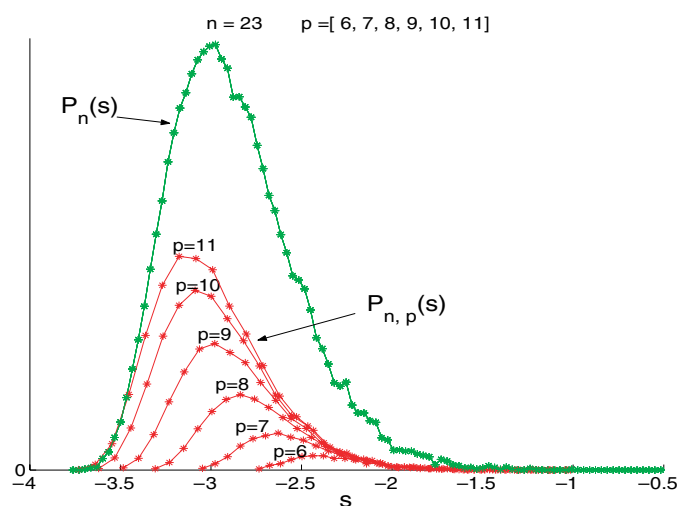


Figure 7. Distributions of actions according to p -families.

therefore their classification into families which share certain properties is conveniently carried out in terms of their codes.

As was shown in section 2.2 the binary code $\{0, 1\}$ is based on the partition of phase space by a vertical line at $x = \frac{1}{2}$ into the two rectangles which are associated with the codes 0 and 1. Only the points of the trajectory which fall in the second rectangle (code 1) contribute to the action, and the increment to the total action per point is $x_i - 1$. Denote by p the number of times the periodic orbit visits the second interval, or equivalently, the number of $v_i = 1$ in the code. The set of all the trajectories which have the same p will be referred to as a ' p -family'. The actions of trajectories within a p -family cluster in substructures which are illustrated in figure 7 in terms of the densities $P_{n,p}(s)$, for $n = 23$ and a few values of p . The $P_{n,p}(s)$ are narrower than $P_n(s)$, and one can show that they are centred about $-\frac{1}{2} \frac{p(n-p)}{n-1}$. Scaling to unit variance and shifting to their mean s value (figure 8), the densities $P_{n,p}(s)$ collapse to a single

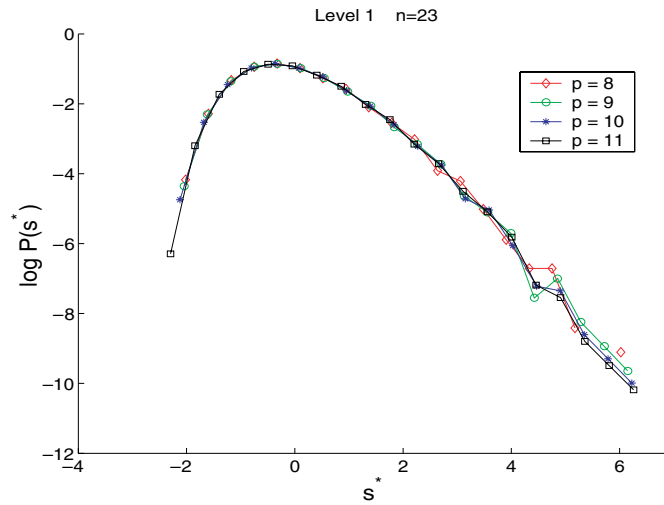


Figure 8. Scaling of the p -family distributions.

function which is very similar to the scaled total density. Thus, the families enable a study of the spectrum of actions with a finer resolution, with an approximate scaling similarity of their densities.

The partition of the actions into p -families is just the first level in a systematic procedure which enables the sorting of the actions according to their codes. The higher the level, the more refined are the resulting families. The higher level families still maintain the scaling similarities, which was discussed for the p -families.

The r th level families, (with $r < n$) are obtained by a partition of phase space into 2^r identical rectangles of unit height, and with $\frac{j-1}{2^r} \leq x < \frac{j}{2^r}$, for all $1 \leq j \leq 2^r$. The family consists of all the n -periodic orbits which go through each of the 2^{r-1} rectangles in the rightmost half of the unit square the same number of times. Given an n -periodic orbit, we denote by $p_l^{(r)}$ the number of times it goes through the l th rectangle with $\frac{l-1}{2^r} \leq x < \frac{l}{2^r}$ and $1 \leq l \leq 2^{r-1}$. A family of the r th level is characterized by the set of 2^{r-1} numbers,

$$\mathbf{P}^{(r)} = \left(p_1^{(r)}, p_2^{(r)}, \dots, p_{2^{r-1}}^{(r)} \right). \tag{35}$$

One can get the \mathbf{P} code by direct inspection of the binary code ν . $p_j^{(r)}$ is the number of times the r digit string, beginning with 1 and terminating with $j - 1$ written in a binary basis, occurs in ν , i.e

$$p_j^{(r)}(\nu) \equiv \# \left(\underbrace{1 \underbrace{00 \dots 01 \dots}_{r \text{ digits}} \dots}_{j-1 \text{ in binary}} \right) \quad \text{in } \nu. \tag{36}$$

One can easily check that the p -families defined at the beginning of this section correspond to $r = 1$, with $p_1^{(1)} \equiv p$. The r and the $r + 1$ partitions are related by

$$p_j^{(r)} = p_{2j}^{(r+1)} + p_{2j-1}^{(r+1)}.$$

Also,

$$\forall r : \sum_{j=1}^{2^{r-1}} p_j^{(r)} = p_1^{(1)} \equiv p.$$

The mean action for a $\mathbf{P}^{(r)}$ family can be written as

$$s_n^{(r)} = \sum_{j=1}^{2^{r-1}} p_j^{(r)} \left(-\frac{1}{2} + \frac{2j-1}{2^{r+1}} \right) = -\frac{p}{2} \left(1 + \frac{1}{2^r} \right) + \frac{p}{2^r} \frac{\sum_{j=1}^{2^{r-1}} j p_j^{(r)}}{\sum_{j=1}^{2^{r-1}} p_j^{(r)}}. \quad (37)$$

Actions which belong to the same family cluster about this mean value within an interval of order $\frac{\sqrt{n}}{2^r}$.

The partition into families breaks the \hat{R} symmetry in the sense that symmetry conjugate pairs of periodic orbits occur in different families. This is clear from the observation that the number of 1 in the two conjugate codes are p and $n-p$. For $r \geq 3$, periodic orbits which are related by \hat{T} can be assigned to different families. (For example, the periodic orbits which are represented by the binary codes (001011) and (001101) are \hat{T} conjugate but they appear in the $r=4$ families (01011000) and (01100100), respectively.) To avoid this problem, one should partition the actions which correspond to the set $\tilde{\mathcal{P}}_n$, where only one representative of each degeneracy class is included (29).

An alternative partitioning of the actions in families can be defined in the following way. Given a binary code ν , let q_1 be the number of 1 in ν , let q_2 be the number of sequences {11} in ν , and in general, q_r is the number of sequences of r consecutive 1 in ν . (Clearly $q_1 = p$.) The r th level family consists of all the n -periodic orbits which have the same $\mathbf{Q}^{(r)}$ code,

$$\mathbf{Q}^{(r)} = (q_1^{(r)}, q_2^{(r)}, \dots, q_r^{(r)}). \quad (38)$$

This partitioning has the advantage that \hat{T} -conjugate orbits are always in the same family, (however, \hat{R} -conjugate orbits are in different families). We found this partitioning more convenient for numerical simulations. The two methods of partitioning, at the same r level, have in common the same resolution 2^{-r} .

The partition of the actions of n -periodic orbits into families provides a very useful tool for the analysis of the spectral correlations, especially because the parameter r which is at our disposal, determines the resolution at which we wish to interrogate the spectrum. Given r , most pairs of actions at a distance less than 2^{-r} belong to the same family, and hence, *intra*-family investigations are sufficient for the study of smaller action differences. However, for larger scales, all actions in a family can be lumped together, and the large range correlations are expressed through the study of *inter*-family correlations. We shall take both approaches when we discuss the two-point correlations in the action spectra.

3.3. An Ising model approach

In the present section, we shall introduce a method to investigate the action spectra on scales which are larger than a given level of resolution. For this purpose, it is convenient to study the Fourier transform of the action distribution, $\hat{P}_n(k)$,

$$\hat{P}_n(k) = \frac{1}{2^n} \sum_{\{v\}} e^{iks_n(v)} = \frac{1}{2^n} \sum_{\{v\}} \exp \left\{ ik \left(\sum_{i,j}^n v_i O_{ij} v_j - \sum_j^n v_j^2 \right) \right\} \quad (39)$$

where the sum is over all possible configurations of the code $\nu = (v_1, v_2, \dots, v_n)$, $v_i \in \{0, 1\}$. The action is given explicitly by

$$s(\nu_n) = \frac{1}{1-2^{-n}} \sum_i \left[\frac{1}{2} v_i^2 + \frac{1}{4} v_i v_{i+1} + \frac{1}{8} v_i v_{i+2} + \dots \right] - \sum_i v_i^2. \quad (40)$$

Formally (39) is the partition sum of a one-dimensional Ising model on a circular lattice with exponentially decreasing interactions and an imaginary temperature. It can be evaluated

using the standard transfer matrix method. Using this method, we can approximate $\hat{P}_n(k)$ by truncating the interaction at any desired range r , $1 \leq r \leq n - 1$. Thus, $r = 1$ is the nearest neighbour approximation, $r = 2$ is the next-to-nearest neighbour approximation etc. When $r = n - 1$ we regain the full range of interactions. The original effective Hamiltonian is invariant under space reflection \hat{R} and time reversal \hat{T} . The invariance under \hat{T} is due to the cyclic property of \hat{O} and hence, is maintained for any truncated version. This is not the case however for the space reflection \hat{R} symmetry. In order to preserve \hat{R} invariance, one has to rescale the strength of the term $\sum_j v_j^2$ which was introduced for \hat{R} invariance of the full action (23). For a given range r of the approximation, the action takes the form

$$s_{n,(r)}(v) = \frac{1}{1 - 2^{-n}} \sum_{\xi=0}^r \sum_{i=1}^n \frac{1}{2^{(\xi+1)}} v_i v_{i+\xi} - \gamma_n(r) \sum_{i=1}^n v_i^2. \tag{41}$$

The symmetry restoring coefficient $\gamma_n(r)$ is calculated by demanding that for the r th order approximation the action be \hat{R} symmetric, i.e. $s_{n,(r)}(v) = s_{n,(r)}(\hat{R}(v))$, and is given by

$$\gamma_n(r) = \frac{1}{1 - 2^{-n}} \sum_{\xi=0}^r \frac{1}{2^{(\xi+1)}} = \frac{1 - (\frac{1}{2})^{r+1}}{1 - (\frac{1}{2})^n}. \tag{42}$$

One recovers $\gamma_n(r) = 1$ for the full range of interactions $r = n - 1$.

This completes the definition of the r th level approximants, and because of the exponential decreasing strength of the interactions we can expect that any quantity computed at the r th level will converge exponentially fast to its full range interaction value.

Note that for the rest of this section we omit the factor $\frac{1}{1-2^{-n}} \approx 1$ which multiplies s_n .

We express $\hat{P}_n(k)$ for a given range r as

$$\hat{P}_n^{(r)}(k) = \frac{1}{2^n} \text{Tr}\{[T^{(r)}(k)]^n\} \tag{43}$$

where the transfer matrix $T^{(r)}(k)$ is given by

$$T^{(r)}(k) = \begin{pmatrix} 1 & 1 & 0 & & & \dots & 0 \\ 0 & 0 & 1 & 1 & 0 & \dots & 0 \\ \vdots & & & & & & \vdots \\ 0 & 0 & & & \dots & 0 & 1 & 1 \\ \beta^{2^r-1} & \beta^{2^r-2} & 0 & & & \dots & 0 \\ 0 & 0 & \beta^{2^r-3} & \beta^{2^r-4} & 0 & \dots & 0 \\ \vdots & & & & & & \vdots \\ 0 & 0 & & & \dots & 0 & \beta & 1 \end{pmatrix} \quad \beta = e^{-i\frac{k}{2^{r+1}}}. \tag{44}$$

Since T depends on powers of β , $\text{Tr}\{[T^{(r)}]^n\}$ is a polynomial in β with real coefficients A_j ,

$$\frac{1}{2^n} \text{Tr}\{[T^{(r)}(k)]^n\} = \sum_{j=0}^{N(n,r)} A_j \beta^j = \sum_{j=0}^{N(n,r)} A_j e^{-ik\frac{j}{2^{r+1}}} \tag{45}$$

where $N(n, r)$ is the degree of the polynomial. Transforming back to $P_n(s)$ yields

$$P_n^{(r)}(s) = \sum_{j=0}^{N(n,r)} A_j^{(r)} \delta\left(s + \frac{j}{2^{r+1}}\right) \tag{46}$$

and

$$\sum_{j=0}^{N(n,r)} A_j^{(r)} = 1. \quad (47)$$

The r th approximant to the action spectrum consists of $N(n,r)$ equally spaced actions $s_j = -\frac{j}{2^{r+1}}$, each weighted by a normalized weight (or probability) $A_j^{(r)}$. The set $\{A_j\}$ contains, together with the spacing $\delta s(n,r) \equiv \frac{1}{2^{r+1}}$, all the information about the statistical properties of the spectrum at the resolution $\frac{1}{2^{r+1}}$. Increasing the range r to $r+1$ results in approximately doubling the number of actions, in addition to distributing them on a lattice with half the spacing. In the limit $r \rightarrow n-1$ (full range interactions) the lattice spacing becomes $\frac{1}{2^n}$ (or $\frac{1}{2^{n-1}}$ taking into account the factor $\frac{1}{1-2^{-n}}$ that was neglected). This observation enables us to connect the present approach with the partitioning of the actions to families according to their codes. The truncation of the interaction at the r th level is approximately equivalent to replacing the actions of all the members of a family by their average value given by (37). Thus, the coefficients $2^n A_j^{(r)}$ approximate the sum of the cardinalities of all the families whose average action is $s_j = -\frac{j}{2^{r+1}}$.

The moments of the distribution are computed using

$$\begin{aligned} \langle s_{n,(r)}^m \rangle &= (-i)^m \left. \frac{\partial^m P_n^{(r)}(k)}{\partial k^m} \right|_{k=0} \\ &= \left(\frac{-1}{2^{r+1}} \right)^m \sum_{j=0}^{N(n,r)} A_j^{(r)} j^m. \end{aligned} \quad (48)$$

The two lowest level approximants can be solved analytically.

$r=1$: the transfer matrix (44) for this 'nearest neighbour interaction' approximation is

$$T^{(r=1)}(k) = \begin{pmatrix} 1 & 1 \\ \beta & 1 \end{pmatrix} \quad \beta = e^{-i\frac{k}{4}}. \quad (49)$$

Its eigenvalues are $\lambda_{\pm} = 1 \pm \sqrt{\beta}$ which yield

$$\begin{aligned} \hat{P}_n^{(r=1)}(k) &= \frac{1}{2^n} [(1 + \sqrt{\beta})^n + (1 - \sqrt{\beta})^n] \\ &= \frac{2}{2^n} \sum_{m=0; \text{even}}^n \binom{n}{m} e^{-ik\frac{m}{8}} \end{aligned} \quad (50)$$

and

$$P_n^{(r=1)}(s) = \frac{2}{2^n} \binom{n}{-8s} \quad (51)$$

with

$$s \in \left\{ 0, -\frac{1}{4}, -\frac{2}{4}, -\frac{3}{4}, \dots, -\frac{1}{4} \left[\frac{n}{2} \right] \right\}.$$

This distribution limits to a Gaussian distribution for large n . The mean and the variance are given by

$$\langle s_{n,(r=1)} \rangle = -\frac{n}{16} \quad \text{var}(s_{n,(r=1)}) = \frac{n}{256}.$$

$r = 2$: the transfer matrix in this ‘next-to-nearest neighbour interaction’ approximation is

$$T^{(r=2)}(k) = \begin{pmatrix} 1 & 1 & 0 & 0 \\ 0 & 0 & 1 & 1 \\ \beta^3 & \beta^2 & 0 & 0 \\ 0 & 0 & \beta & 1 \end{pmatrix} \quad \beta = e^{-i\frac{k}{8}}. \quad (52)$$

The eigenvalues of $T^{(r=2)}$ are

$$\lambda_{1\pm} = \frac{1}{2}(1 - \beta \pm \sqrt{\Delta_1}) \quad \lambda_{2\pm} = \frac{1}{2}(1 + \beta \pm \sqrt{\Delta_2})$$

with $\Delta_1 = 1 + 2\beta - 3\beta^2$; $\Delta_2 = 1 - 2\beta + 5\beta^2$. This gives

$$\hat{P}_n^{(r=2)}(k) = \frac{2}{2^{2n}} \sum_{m=0; \text{even}}^n \sum_{j=0}^{n-m} \sum_{u=0}^{\frac{m}{2}} \sum_{t=0}^{\frac{m}{2}-u} \left[\binom{n}{m} \binom{n-m}{j} \binom{\frac{m}{2}}{u} \binom{\frac{m}{2}-u}{t} C_{jtu} e^{-ik\frac{j+t+2u}{8}} \right] \quad (53)$$

with

$$C_{jtu} = 2^t \{3^u (-1)^{j+u} + 5^u (-1)^t\}.$$

The action distribution is

$$P_n^{(r=2)}(s) = \frac{2}{2^{2n}} \sum_{m=0; \text{even}}^n \sum_{j=0}^{n-m} \sum_{u=0}^{\frac{m}{2}} \left[\binom{n}{m} \binom{n-m}{j} \binom{\frac{m}{2}}{u} \binom{\frac{m}{2}-u}{-8s-2u-j} C_{ju}(s) \right] \quad (54)$$

with

$$C_{ju}(s) = 2^{-8s-2u-j} \{3^u (-1)^{j+u} + 5^u (-1)^{-8s-j}\}.$$

The action takes the values

$$s \in \left\{ 0, -\frac{1}{8}, -\frac{2}{8}, -\frac{3}{8}, \dots, -\frac{n}{8} \right\}$$

and the summation coefficients u, j, m must fulfil the conditions

$$2u + j \leq -8s \leq u + j + m/2$$

to keep the binomial coefficients well defined. The $r = 2$ distribution is not Gaussian, its mean, variance and third moment can be computed by a straightforward but cumbersome calculation:

$$\langle s_{n,(r=2)} \rangle = -\frac{n}{16} \left(1 + \frac{1}{2} \right) \quad \text{var}(s_{n,(r=2)}) = \frac{n}{256} \left(1 + \frac{1}{4} \right)$$

$$\langle (s_{n,(r=2)} - \langle s_{n,(r=2)} \rangle)^3 \rangle = \frac{3n}{4096}.$$

We were unable to compute analytically the action distributions at higher levels, since this involves finding the eigenvalues of the 2^r -dimensional transfer matrices. However, the computation can be performed using computer codes which perform algebraic manipulations. For any r and β one can compute $\text{Tr}\{[T^{(r)}(k)]^n\}$ by raising $T^{(r)}$ to the power n and taking the trace. Using Newton’s identities, one can compute the coefficients of the characteristic polynomial of $T^{(r)}$ from the traces of its lower powers, $\text{Tr}\{[T^{(r)}(k)]^l\}$, $l = 1, \dots, 2^r$. The traces of higher powers can then be expressed recursively in terms of these coefficients. This way we were able to perform computations up to the level $r = 9$, without reaching the limits of our computer resources.

At the beginning of the section, we argued that due to the exponential decrease of the interactions, computing any quantity at a given level r converges exponentially fast to the full $r = n - 1$ calculation. Thus, it can be expected that any quantity of interest will be given by

a geometric series in 2^{-r} . Knowing the first two levels ($r = 1, 2$) may allow us to extrapolate and obtain the leading terms for $r = n - 1$. Applying this strategy for the first three moments, we obtained the expressions

$$\langle s_{n,(r)} \rangle = -\frac{n}{8} \left(1 - \frac{1}{2^r} \right) \longrightarrow -\frac{n}{8} \quad (55)$$

$$\text{var}(s_{n,(r)}) = \frac{n}{192} \left(1 - \frac{1}{4^r} \right) \longrightarrow \frac{n}{192} \quad (56)$$

$$\langle (s_{n,(r)} - \langle s_{n,(r)} \rangle)^3 \rangle = \frac{n}{768} \left(1 - \frac{1+3r}{4^r} \right) \longrightarrow \frac{n}{768}. \quad (57)$$

These expressions were checked by comparing them to the computer aided, large r calculations. This computation indicates that the truncation error introduced at the r th level is of order 2^{-r} .

We shall return to the results of the Ising model when we discuss the pair correlations in the action spectrum which is the subject of the next section.

4. Pair correlations in the action spectrum

So far we have discussed the *distribution* of actions. Now we turn to study their *pair correlations*, which is the main issue of the present work. We examine whether the classical action spectrum exhibits correlations, and whether these correlations conform with the semiclassical theory which was presented in section 1.

There are two distinct length scales in any discrete and finite spectrum: the width or support of the distribution on the largest scale and the nearest neighbour spacing on the smallest scale. The fact that the support is finite induces a trivial correlation: the probability of finding two points separated by a distance larger than the range of the support is zero. The nearest neighbour scale is of great interest, in particular for ‘rigid’ spectra such as the quantum spectra of classically chaotic systems. They exhibit *level repulsion* as predicted by RMT, i.e. the probability of finding two nearest neighbours at distance δ vanishes as $\delta \rightarrow 0$. We have already hinted in section 1 that the pair correlations in the action spectrum are expected on a scale which is much larger than the mean spacing.

We shall perform the analysis of pair correlations in several steps. First, we shall examine the correlations on the scale of the mean level spacing. We shall show that the m th nearest neighbour spacing distributions are consistent with the corresponding Poisson distributions, as long as m is smaller than the correlation length measured in units of the mean spacing. We shall then study the form factor of the pair correlation function, and compute it in various ways. The main result of this investigation is that the correlations exist, and their scaling with n agrees with the semiclassical expectations.

4.1. The m th neighbour spacing distributions

The m th neighbour spacing distribution $p^{(n)}(\sigma; m)$ is a straightforward generalization of the widely used nearest neighbour spacing distribution. To define this distribution, the action spectrum is ordered so that $s_i < s_{i+1}$, degeneracy sets are represented by a single value and the spectrum is normalized by the nearest neighbour spacings

$$\langle \Delta s^{(n)} \rangle \simeq \frac{2}{3} \frac{n^2}{2^n}. \quad (58)$$

Then $p^{(n)}(\sigma; m)$ is the probability that $\frac{s_{i+m} - s_i}{\langle \Delta s^{(n)} \rangle}$ takes the value σ .

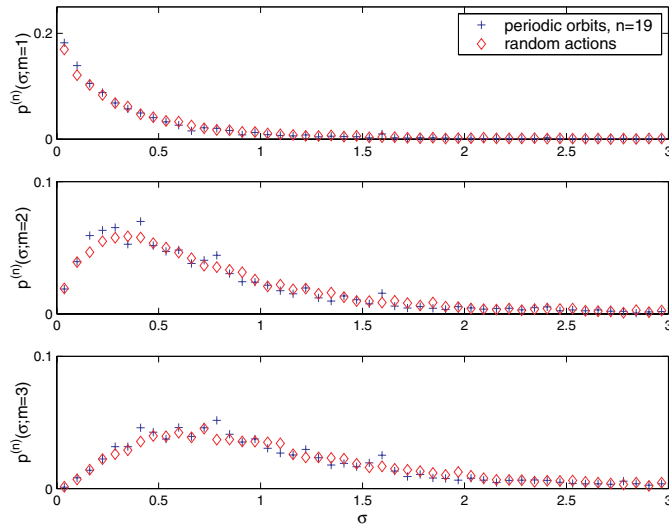


Figure 9. The first, second and third neighbour distributions ($n = 19$).

As a reference spectrum, we generated numerically a Poissonian spectrum. It is randomly chosen from a Gaussian probability density which has the same mean, variance and degeneracy structure as the action spectrum for the n value of interest. In the upper frame of figure 9 the nearest neighbour distribution, $p^{(n)}(\sigma; m = 1)$, for $n = 19$ is plotted together with the random (Poissonian) nearest neighbour distribution. The similarity between the two distributions, which persists over six orders of magnitude, provides strong evidence in favour of the claim that on the mean spacing scale, the action spectrum is statistically random.

This finding is further corroborated in the lower frames of figure 9 where the spacing distributions for $m = 2, 3$ are compared with the corresponding random distributions.

To go even further in m , we studied numerically the summed distributions

$$p_M^{(n)}(\sigma) = \sum_{m=1}^M p^{(n)}(\sigma; m) \tag{59}$$

which approximate the two point correlation function $R_{2;n}(\sigma) = p_\infty^{(n)}(\sigma)$ in the range $0 < \sigma < M$.

Figure 10 shows $p_M^{(n)}(\sigma)$ for $M = 20, 50, 100, n = 19$ together with the corresponding random distributions. These values M should be compared with the correlation length expected to be of order

$$\sigma_{\text{corr}} \approx \frac{1/n}{\langle \Delta S^{(n)} \rangle} = 3 \frac{2^{n-1}}{n^3} \quad (\approx 90 \text{ for } n = 19). \tag{60}$$

This numerical investigation clearly demonstrates that the systematic deviation between the random and the actual distributions increases as M approaches the correlation length.

4.2. The classical spectral form factor

The purpose of the present section is to study the form factor of the classical action spectrum (13). We start by investigating alternative methods for averaging the form factor, the need for which and the difficulties involved were discussed at length in section 1. We shall study

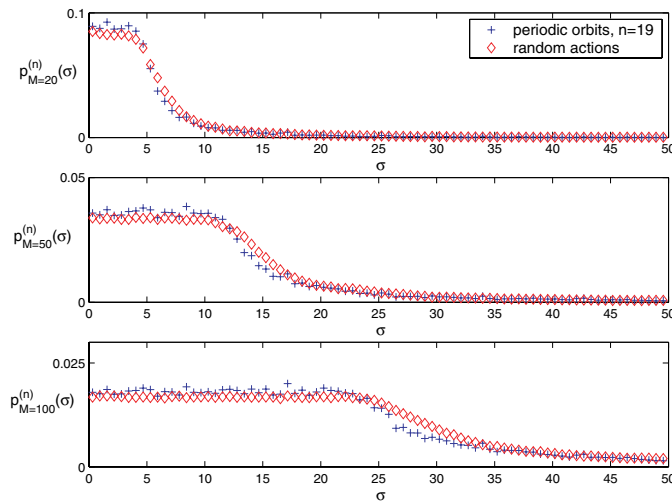


Figure 10. Integrated distributions with $M = 20, 50, 100, n = 19$.

the function $\mathcal{K}_n(k)$ (17), and in particular test whether the action spectrum of the Baker map satisfies either of the equivalent relations,

$$\mathcal{K}_n(k) \approx \frac{k}{2\pi n} K_{\text{RMT}}\left(\frac{2\pi n}{k}\right) \quad \text{or} \quad \tau \mathcal{K}_n\left(\frac{2\pi n}{\tau}\right) \approx K_{\text{RMT}}(\tau). \quad (61)$$

Since the Baker map is invariant under time reversal, the appropriate RMT expression is that for the circular orthogonal ensemble (COE) $K_{\text{COE}}(2\tau)$, where the factor 2 in the argument is due to the invariance of the Baker map under the \hat{R} symmetry. The explicit expression for $K_{\text{COE}}(\tau)$ is given by

$$K_{\text{COE}}(\tau) = \begin{cases} 2\tau - \tau \ln(1 + 2\tau) & \text{for } \tau < 1 \\ 2 - \tau \ln\left(\frac{2\tau+1}{2\tau-1}\right) & \text{for } \tau > 1. \end{cases} \quad (62)$$

Before applying any averaging, the function $\tau \mathcal{K}_n\left(\frac{2\pi n}{\tau}\right)$ displays strong fluctuations which are shown in figure 11 for $n = 15$ together with the expected COE result. The large fluctuations make the comparison quite meaningless, and the figure is shown to emphasize the need for averaging.

Using the running average,

$$\bar{f}(x) = \frac{1}{x} \int_0^x f(y) \, dy \quad (63)$$

the large fluctuations are reduced, and the curve labelled ‘periodic orbits’ in figure 12 is the running average obtained by computing the form factor from the set of $n = 17$ periodic orbits. The agreement with the corresponding COE curve persists up to $\tau \approx 0.5$. The line marked ‘diag’ is the curve obtained by assuming that the actions are not correlated, and it agrees very well with the line marked as ‘rand’ which was computed for the random set of actions (see section 4.1). The difference between the data and the random curves is a clear indication of the presence of correlations, whose similarity to the predicted COE result goes beyond the leading ‘diagonal’ approximation. The running average procedure is not satisfactory, because it is practical only for low values of n . As n increases, the number of periodic orbits proliferates exponentially, and the fluctuations in the form factor grow

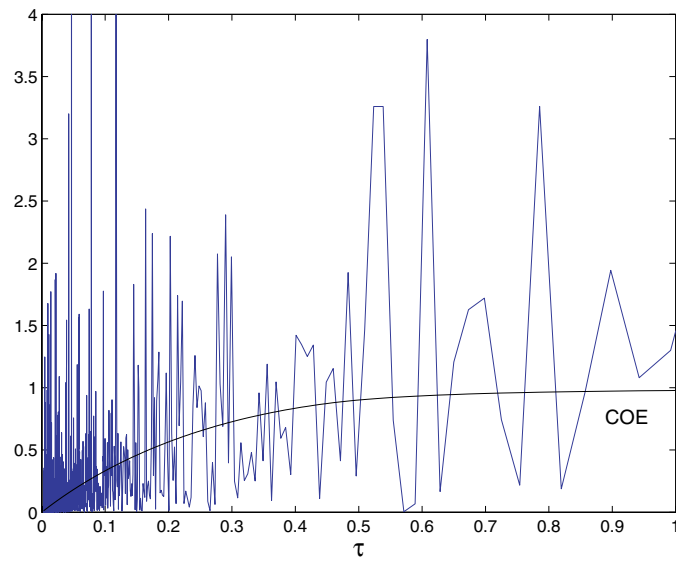


Figure 11. The function $\tau \mathcal{K}_n\left(\frac{2\pi n}{\tau}\right)$ ($n = 15$) (61) and the RMT prediction.

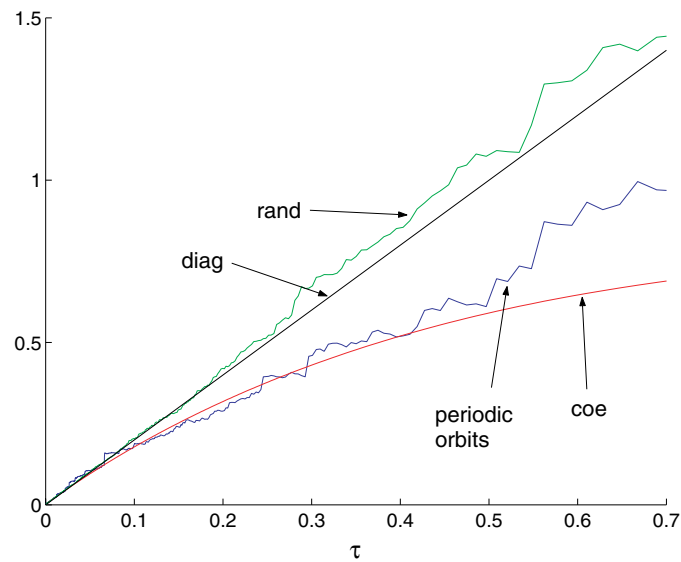


Figure 12. A running average (63) of $\tau \mathcal{K}_n\left(\frac{2\pi n}{\tau}\right)$ ($n = 17$).

as rapidly. Moreover, this method does not help to unravel the dynamical origin of the correlations.

A systematic averaging procedure, which can be applied for any n , uses the concept of families which was introduced in section 3.2. The spectrum of actions of n -periodic orbits is partitioned to families at the r th level with labels $\mathbf{P}^{(r)}$ (see (35)). As long as r is sufficiently small such that 2^{-r} is larger than the correlation length, only *intra*-family correlations are important. The form factor can be approximated by an incoherent sum over the form factors

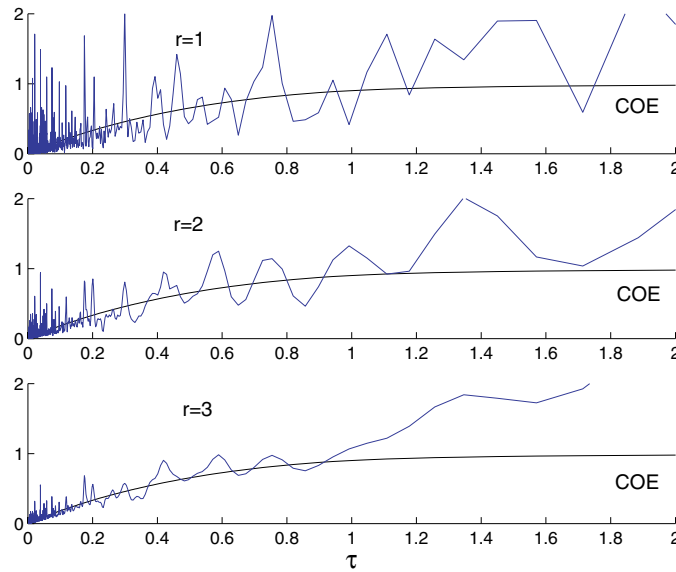


Figure 13. $\mathbf{P}^{(r)}$ family averaged $\tau \mathcal{K}_n \left(\frac{2\pi n}{\tau} \right)$ for $r = 1, 2, 3, n = 15$.

which pertain separately to orbits within one family:

$$\mathcal{K}_n^{(r)}(k) = \frac{1}{N_n} \sum_{\mathbf{p}^{(r)}} \left| \sum_{a \in \mathbf{p}^{(r)}} e^{iks_a^{(n)}} \right|^2. \tag{64}$$

Each family of actions is supported on an interval of size which decreases with r as 2^{-r} . Hence from the requirement $k\Delta s > 2\pi$ we deduce $N > 2^r$, and the range of values of τ which can be described by this method is bounded from above by $\approx \frac{n}{2^r}$. Thus by increasing r , we gain a higher level of smoothing, but we lose on the range of τ where this method can be used.

The resulting form factors for $n = 15$ and $r = 1, 2, 3$ are shown in figure 13. It shows that the smoothing gets more effective as r increases, without appreciable loss of correlations in the interval $0 < \tau < 1$. This is consistent with the expectation that the spectral correlation length is $\frac{1}{15}$, which is smaller than the family separation of $\approx 2^{-r}$ for the values $r = 1, 2, 3$. A closer comparison of the $r = 2$ and $r = 3$ curves near $\tau = 1$ shows that the deviations from the RMT prediction start earlier for the $r = 3$ data. To investigate this trend further, we use the $\mathbf{Q}^{(r)}$ partitioning (38) which is more convenient from the numerical point of view. It allows us to extend the level further, and the data for $r = 4, 5$ are shown in figure 14. Since now the family range is smaller than $\frac{1}{n}$, the correlations can be studied only on a lower range of τ values. This, and similar other numerical investigations provide strong evidence in support of the $\frac{1}{n}$ dependence of the correlation length, in agreement with the semiclassical expectations.

As was commented previously, the partition into families breaks pairs of \hat{R} -conjugate orbits. Hence, the RMT expression which is used in figures 13 and 14 is $K_{\text{COE}}(\tau)$ and not $K_{\text{COE}}(2\tau)$ which is used for the comparison with the full dataset.

The Ising model approach (3.3) offers a complementary view of the form factor. As was explained in (3.3), the truncation at the r th level does not allow us to distinguish between actions which are within 2^{-r} , and counts them as if they are degenerate. Thus, the only way in which we can get spectral information on the scale of $\frac{1}{n}$ in this model is to use r such

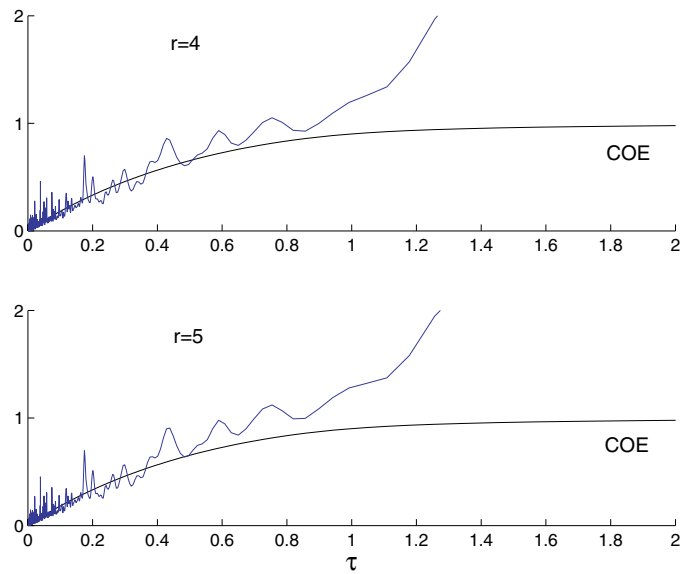


Figure 14. $Q^{(r)}$ family averaged $\tau \mathcal{K}_n \left(\frac{2\pi n}{\tau} \right)$ for $r = 4, 5, n = 15$.

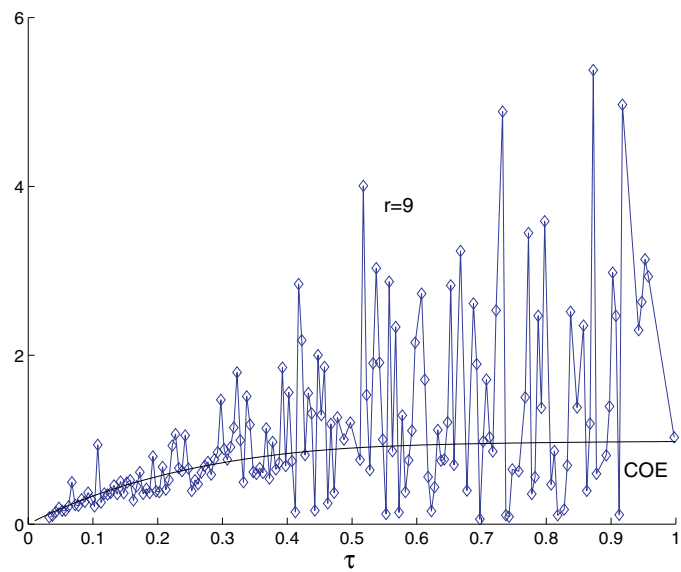


Figure 15. $\tau \mathcal{K}_n \left(\frac{2\pi n}{\tau} \right)$, from the Ising model with $r = 9$, averaged over $17 \leq n \leq 22$.

that $\frac{1}{n} \gg 2^{-r}$. The spectral correlations are now studied as correlations *between* degeneracy groups, rather than *within* a group. Figure 15 shows the average of a few form factors, corresponding to values of n from $n = 17$ to $n = 22$, given by the model with $r = 9$ which satisfies the criterion above. The average over n reduces the fluctuations of the form factor so it is possible to compare it directly to the RMT.

The fact that the action spectrum is resolved with an accuracy of 2^{-r} sets a lower limit to the values of τ which are accessible by the model, which is $\tau_{\min} \approx \frac{n}{2^r}$. This is why the low τ values in figure 15 are absent.

5. Discussion

The semiclassical predictions which were presented in section 1 were checked in detail and were found to be well satisfied for the Baker map. They consist of the following main points:

- The action spectrum shows pair correlations which are universal and consistent with the predictions of the semiclassical theory and RMT.
- The correlation length is of order $\frac{1}{n}$ which exceeds the mean spacing by a factor which grows exponentially with n . The spectrum of actions is Poissonian on smaller scales.
- The correlations can be associated with families of periodic orbits which have a similar dynamical structure that can be associated systematically with their symbolic codes.

Various aspects of these points were confirmed for other systems [2, 3, 6, 7, 10]. The results of [7, 10] are unique, because the phase space of the mapping considered is four dimensional, and the semiclassical theory predicts that the action correlation range scales with n as $\frac{1}{n^2}$. This scaling was confirmed.

Richter and Sieber [12] pointed out the pairs of periodic orbits which provide the correlations that are necessary for the second-order term in the small τ expansion of the form factor. These orbits spend about half of their time quite close to each other, and the rest of the time they go along the time-reversed part of their partner's orbit. This way both orbits visit the same parts of phase space, but the order in which they do it is different. Similar pairs were also proved to provide the answer in the case of quantum graphs [14]. The families which we have identified here as storing the correlations between the actions are of the same nature, but of a more general character. They do not rely exclusively on pairs conjugated partially by time reversal (as explained above), but by the requirement that the correlated members spend the same amount of time in the same subdomains of phase space. This definition of families is also consistent with the work of [7], where the periodic orbits in a family follow the same segments of phase space which were related to each other by symmetries other than time reversal. Because of the strong link between phase space partition and symbolic codes, it was possible to characterize the families by a common code. Unfortunately, even with this tool, we were not able to derive the classical correlation function using classical arguments only. This remains an enigma which should be addressed. At the same time, one should also be able to show that the spectrum of actions on smaller scales is Poissonian. This is assumed, but not discussed, in [12, 14].

In the present paper, we focussed our attention on discrete maps and their periodic orbits. However, most systems of interest are Hamiltonian flows, where the time is a continuous variable, and the quantum spectrum is on the real line and not on the unit circle. This does not pose any essential problem, since several quantization techniques make use of an auxiliary map to derive the quantum energies, and it was shown that for chaotic systems, the spectral statistics of the energies and of the eigenphases of the auxiliary map are the same in the semiclassical limit [5, 26, 27]. A more direct approach was recently introduced in [28], where the quantization of the Hamiltonian flow is carried out in terms of a quantum map which evolves the system along a sequence of equally spaced times $t_n = n\Delta t$. The semiclassical expression for the spectral form factor is analogous to (7), and the periodic orbits have periods which are integer multiples of Δt and their energies are restricted to a well-defined energy interval.

Integrable dynamics lead to Poissonian spectra [29]. In the present context, this implies that the actions are Poissonian also [7]. Recently, it was shown in [30] that in order to account for finer spectral correlations which are due to the spectrum being pure point, finer correlations must exist, but this discussion exceeds the scope of the present paper.

Acknowledgments

We would like to acknowledge discussions with and comments from Herve Kunz, Gergely Palla and Jean-Luc Helfer. The work was supported by the Minerva Center for Physics of Complex Systems and by grants from the Israel Science Foundation and the Minerva Foundation.

References

- [1] Bohigas O 1989 *Random Matrix Theories and Chaotic Dynamics* Les Houches, session LII (Amsterdam: Elsevier)
- [2] Argaman N, Dittes F M, Doron E, Keating J P, Kitaev A Y, Sieber M and Smilansky U 1993 *Phys. Rev. Lett.* **71** 4326–9
- [3] Dittes F M, Doron E and Smilansky U 1994 *Phys. Rev. E* **49** 963–6
- [4] Aurich R and Sieber M 1994 *J. Phys. A: Math. Gen.* **27** 1967–79
- [5] Smilansky U 1995 *Semiclassical Quantization of Chaotic Billiards—a Scattering Approach* Les Houches, session LXI (Amsterdam: Elsevier)
- [6] Tanner G 1999 *J. Phys. A: Math. Gen.* **32** 5071–85
- [7] Cohen D, Primack H and Smilansky U 1998 *Ann. Phys., NY* **264** 108–70
- [8] Sano M M 2000 *Chaos* **10** 195–210
- [9] Gutzwiller M C 1982 *Physica D* **5** 183
- [10] Primack H and Smilansky U 2000 *Phys. Rep.* **327** 1, 2
- [11] Harayama T and Shudo A 1992 *J. Phys. A: Math. Gen.* **25** 4595
- [12] Sieber M and Richter K 2001 *Phys. Scr.* **90** 128
- [13] Braun P A, Haake F and Heusler S 2002 *J. Math. Phys.* **35** 1381
- [14] Berkolaiko G, Schanz H and Withney R 2002 *Phys. Rev. Lett.* **82** 104101
- [15] Smilansky U 2002 Semiclassical quantization of maps and spectral correlations *Supersymmetry and Trace Formulae: Chaos and Disorder* ed I V Lerner, J P Keating and D E Khmelnitskii (New York: Kluwer/Plenum) pp 173–92
- [16] Goldstein H 1957 *Classical Mechanics* (Reading, MA: Addison-Wesley)
- [17] Saraceno M 1990 *Ann. Phys., NY* **199** 37–60
- [18] Balazs N L and Voros A 1989 *Ann. Phys., NY* **190** 1–31
- [19] Saraceno M and Voros A 1994 *Physica D* **79** 206–68
- [20] Dittes F M and Doron E Private communication
- [21] Berry M V 1985 *Proc. R. Soc. A* **400** 229–51
- [22] Primack H and Smilansky U 1998 On the accuracy of the semiclassical trace formula *J. Phys. A: Math. Gen.* **31** 6253–77
- [23] Hannay J H and Ozorio De Almeida M 1984 *J. Phys. A: Math. Gen.* **17** 3429–40
- [24] Sinai Y 1990 *Geometric Aspects of Functional Analysis (Lecture Notes in Math vol 1469)* (Berlin: Springer) pp 41–59
- [25] Ozorio De Almeida M and Saraceno M 1991 *Ann. Phys., NY* **210** 1–15
- [26] Bogomolny E B 1992 *Nonlinearity* **5** 805
- [27] Doron E and Smilansky U 1992 *Nonlinearity* **5** 1055
- [28] Eckhardt B and Smilansky U 2001 *Found. Phys.* **31** 543–56
- [29] Berry M V and Tabor M 1976 *Proc. R. Soc. A* **349** 101–23
- [30] Bogomolny E 1999 Action correlations in integrable systems *Preprint chao-dyn/9910036*